

Article

Hydrofluoric Acid-Free Synthesis of MIL-101(Cr)-SO₃H

Tamara M. Bernal, Fernando Rubiera  and Marta G. Plaza * 

Instituto de Ciencia y Tecnología del Carbono (INCAR), CSIC, C/Francisco Pintado Fe 26, 33011 Oviedo, Spain; tamara.bernal@incar.csic.es (T.M.B.); frubiera@incar.csic.es (F.R.)

* Correspondence: m.g.plaza@incar.csic.es

Abstract: The conventional synthesis of the Metal–Organic Framework (MOF) MIL-101(Cr)-SO₃H employs hydrofluoric acid as the modulator, posing handling challenges due to its irritating, corrosive, and toxic nature, as well as its reactivity with glass and metals. This study aims to find a new hydrofluoric acid-free synthesis route for MIL-101(Cr)-SO₃H, proposing acetic acid and nitric acid as modulator alternatives. Four MIL-101(Cr)-SO₃H samples were prepared: one without any modulator and the other three using a similar volume of either hydrofluoric acid, acetic acid, or nitric acid as the modulator. The so-obtained mass yield ranked as follows: without any modulator (32.6%) > acetic acid (29.6%) > nitric acid (25.2%) >> hydrofluoric acid (2.2%), whereas the total pore volume and BET surface area followed the order: hydrofluoric acid (0.87 cm³ g⁻¹, 1862 m² g⁻¹) > nitric acid (0.81 cm³ g⁻¹, 1554 m² g⁻¹) > acetic acid (0.72 cm³ g⁻¹, 1374 m² g⁻¹) > without any modulator (0.69 cm³ g⁻¹, 1342 m² g⁻¹). Despite the superior texture parameters obtained using hydrofluoric acid, the low synthesis yield and associated risks make this route non-viable. Acetic or nitric acid-based synthesis offers a promising alternative with a drastically higher yield, safer handling, and reduced environmental impact. In an attempt to improve the textural properties of the hydrofluoric acid-free MOFs, a series of samples were produced with increasing amounts of acetic acid, achieving BET surface areas of up to 1504 m² g⁻¹ and pore volumes of up to 0.81 cm³ g⁻¹.

Keywords: MIL-101(Cr)-SO₃H; MOF; modulator; synthesis



Citation: Bernal, T.M.; Rubiera, F.; Plaza, M.G. Hydrofluoric Acid-Free Synthesis of MIL-101(Cr)-SO₃H. *Crystals* **2024**, *14*, 411. <https://doi.org/10.3390/cryst14050411>

Academic Editor: Ferdinando Costantino

Received: 2 April 2024
Revised: 22 April 2024
Accepted: 24 April 2024
Published: 27 April 2024



Copyright: © 2024 by the authors. Licensee MDPI, Basel, Switzerland. This article is an open access article distributed under the terms and conditions of the Creative Commons Attribution (CC BY) license (<https://creativecommons.org/licenses/by/4.0/>).

1. Introduction

Metal–Organic Frameworks (MOFs) represent an advanced category of microporous materials characterized by elevated surface area and porosity [1]. They were classified by the International Union of Pure and Applied Chemistry (IUPAC) as a subgroup within coordination polymers (CPs) characterized by the presence of “potential voids” [2]. These frameworks are created through the covalent or ionocovalent bonding of metal ions or clusters with polyfunctional organic molecules, forming infinite two- or three-dimensional networks [3,4]. MOFs have become a thriving area in materials science and engineering, largely due to the adaptability of their structures, which can be precisely tailored through careful control of the assembly process [2]. The strategic pairing of metal atom centers with diverse organic ligands results in a material with a customizable pore size and a range of distinctive physicochemical properties [5].

The crystallization, structure, and morphology of MOFs are influenced not solely by the building blocks’ characteristics but also by various synthetic conditions. These conditions encompass factors such as the type of solvent, pH level in the reaction mixture, temperature, concentration of the reagents, molar ratio of the starting materials, existence of counter ions, and pressure. These factors exert a significant influence on the structural chemistry of ligands and the assembly process, resulting in the generation of products exhibiting a variety of structures [6]. These unique attributes make MOFs suitable for a broad spectrum of potential applications across various sectors, including but not limited to adsorption [7–10], catalysis [11–14], and heat transformation [15,16].

The materials developed by the Lavoisier Institute (MIL) represent an extensively explored category in the field of MOFs. Specifically, MOFs built on M(III) terephthalates (where M = Cr, Al, Mn, among others), along with terephthalate derivatives, constitute an important subclass of MOFs. These materials hold a prominent position among acknowledged MOF types, especially in terms of their potential applications. Among these, the MIL-101 series MOFs share a common zeolite topology but differ in surface morphology, density, and pore size [5]. MIL-101(Cr) is noteworthy as a representative material within the MIL series and stands as one of the most thoroughly researched MOFs to date. Its stability across a range of pH conditions, along with a high surface area and a dense concentration of open metal sites, contributes to its prominence in ongoing research efforts [17,18]. In this sense, hydrothermal synthesis is broadly used to synthesize this MOF due to its numerous advantages, including mild operational conditions (with reaction temperatures typically below 300 °C), one-pot synthesis procedure, environmental friendliness, and effective dispersion in solution [19,20]. Furthermore, the hydrothermal method offers significant control over grain size, crystalline phase, particle morphology, and surface chemistry by adjusting parameters such as solution composition, reaction temperature, pressure, solvent properties, additives, and aging duration [21]. In particular, MIL-101(Cr)-SO₃H exhibits notable thermal and chemical stability across diverse environmental conditions, encompassing exposure to air, aqueous solutions, and variations in acidity levels. The inherent robustness of the material, coupled with the strong Brønsted acid characteristics associated with the -SO₃H group, establishes it as a highly promising candidate for subsequent modifications in scientific applications [22]. The inclusion of negatively charged -SO₃H groups presents additional adsorption sites.

A modulator is frequently added during the synthesis of MOFs to improve their adsorption capacity by (i) increasing both their specific surface area and pore volume, generating more sorption sites due to missing linkers; (ii) influencing the nucleation behaviors; and (iii) controlling the particle size of MOFs [23].

The standard procedure to synthesize MIL-101(Cr)-SO₃H comprises the reaction of Monosodium 2-Sulfoterephthalate with nonahydrated chromium nitrate, employing hydrofluoric acid as the modulator and water as the solvent [22,24]. However, despite the fact that hydrofluoric acid is commonly employed as a mineralizing agent to enhance the synthesis efficiency and crystal size of MOFs, its utilization is discouraged due to its classification as a hazardous chemical with high corrosiveness and tissue-penetrating properties, posing severe health risks including life-threatening poisoning. Consequently, extreme caution must be exercised when handling hydrofluoric acid, necessitating the use of protective gear and safety measures exceeding those required for other mineral acids [2,25]. Alternative synthesis methods make use of hydrochloric acid as the modulating agent but require either extended reaction times [26] and/or raising the reaction temperature [27], which results in elevated energy consumption and higher production costs. Therefore, the aim of this study is to find a new synthesis route for MIL-101(Cr)-SO₃H, free of hydrofluoric acid. In this context, two alternative modulators, namely acetic acid and nitric acid, were explored due to their lower toxicity and reduced corrosive properties.

2. Materials and Methods

2.1. Chemicals and Reagents

Chromium (III) nitrate nonahydrate was supplied by Thermo Scientific ($\geq 99.99\%$ metals basis). Monosodium 2-Sulfoterephthalate was purchased from TCI Europe ($\geq 98\%$ by HPLC, titration analysis). Hydrofluoric acid (40%) and anhydrous methanol ($\leq 0.003\%$ H₂O) were obtained from Supelco. Acetic Acid (glacial) was purchased from EMSURE. Nitric acid (65%) was supplied by J.T. Baker. N,N-Dimethylformamide (DMF, $\leq 0.015\%$ H₂O) and acetone ($\geq 99.8\%$) were obtained from VWR Chemicals. Hydrochloric acid (37%) was purchased from Panreac. All reagents were used as received, without further treatment. Ultra-high-purity (99.999%) He and N₂ were used to characterize the samples by gas physisorption.

2.2. Synthesis of MIL-101(Cr)-SO₃H

Samples were synthesized according to previously reported hydrothermal synthesis with some modifications [22]. Briefly, 2.0 g (5 mmol) of chromium (III) nitrate nonahydrate, 2.7 g (10 mmol) of Monosodium 2-Sulfoterephthalate and 0.3 mL of modulator were added to 30 mL of deionized water. This mixture was sonicated to dissolve the solids and then transferred to a Teflon-lined stainless steel reactor (Parr, model 4744) and heated at 190 °C for 24 h. The resulting green powder was then isolated by centrifugation and subsequently washed with deionized water and methanol, in the case of the sample prepared using hydrofluoric acid, or with hot deionized water, DMF and acetone, in the remaining cases, to obtain MIL-101(Cr)-SO₃Na. The latter solid was post-synthetically acidified in 60 mL of dilute hydrochloric acid 0.08 M, prepared with 150 mL of methanol, 150 mL of deionized water and 2 mL of concentrated hydrochloric acid, at 80 °C overnight, to obtain MIL-101(Cr)-SO₃H. The acidified framework was washed with hot deionized water and acetone to finally be heated under vacuum at 120 °C for 12 h.

2.3. Characterization of MIL-101(Cr)-SO₃H Samples

The chemical composition of the synthesized MOFs was examined by the elemental analysis of the dried MOFs at 105 °C for 1–2 h in a CHNS-932 analyzer and a VTF-900 analyzer from LECO.

Surface chemistry was evaluated by Fourier-transform infrared (FT-IR) spectroscopy. The FT-IR spectra of the MOFs were recorded by a Nicolet 8700 spectrometer in the region of 4000–400 cm⁻¹ using a Smart Orbit diamond attenuated total reflectance (ATR) accessory. OMNIC Software (version 8.3) from Thermo Scientific was employed for the analysis of the obtained spectra.

The morphology of the samples was investigated through scanning electron microscopy (SEM). SEM images were obtained using a Quanta 650 FEG instrument, from FEI company, equipped with an S/TEM detector. Optimal conditions for non-conductive samples were used: low-vacuum and a secondary electron large-field detector (LFD). Additionally, the surface of the MOFs was coated with an ultra-thin film of Ir to prevent the charging of the MOFs during the SEM measurements.

The crystallinity of the samples was investigated through powder X-ray diffraction (PXRD) analysis. PXRD spectra were collected on a D5000 diffractometer from Siemens, operating at 40 kV and 20 mA, using Cu-K α radiation.

Thermogravimetric analyses (TGAs) were performed to analyze the thermostability of the samples. TG curves were acquired subjecting ca. 10 mg of sample to a heating rate of 10 °C min⁻¹ under a nitrogen flow rate of 50 cm³ min⁻¹ in a TGA 92 thermogravimetric analyzer from SETARAM.

The porous texture of the samples was analyzed by gas physisorption. The N₂ adsorption and desorption isotherms at –196 °C were measured using a automated manometric adsorption analyzer, Micro 100, from 3P Instruments. The pore size distribution (PSD) and the total pore volume were estimated using the non-local density functional theory (NLDFT) method, making use of the SAIEUS Program (version 3.0) and the Zeolite(H-Form)-N2-77, NLDFT, Cylindrical model, optimally minimizing the second derivative (“roughness”) of the calculated distribution via the L-curve method, which provided the best fit to the experimental data. The apparent surface area was calculated using the Brunauer–Emmett–Teller (BET) method following the IUPAC recommendations [28] and the observations of Rouquerol and co-workers [29].

3. Results and Discussion

3.1. The Effect of the Type of Modulator Used in the Synthesis of MIL-101(Cr)-SO₃H

Table 1 shows the elemental analysis obtained for the MIL-101(Cr)-SO₃H MOFs synthesized in this work without any modulator and using either hydrofluoric acid, acetic acid, or nitric acid as the modulator. The chemical formula of MIL-101(Cr)-SO₃H is {Cr₃(H₂O)₃O[(O₂C)–C₆H₃(SO₃H)–(CO₂)₂]₂[(O₂C)–C₆H₃(SO₃)–(CO₂)]}·nH₂O [26], from

which the calculated elemental composition results: 16.3 wt.% Cr, 30.1 wt.% C, 1.8 wt.% H, 41.8 wt.% O, and 10.0 wt.% S. As can be seen in Table 1, the carbon content of all the samples is close to the stoichiometric value, with the MOF synthesized using acetic acid as the modulator being the closest (only 1% deviation; 0.2 percentage points). The oxygen content of the four samples also matches the expected value, and again, the MOF synthesized making use of acetic acid is the closest, with just a 3% deviation (1.4 percentage points). On the other hand, the highest deviation from the stoichiometric content of carbon and oxygen was obtained for the MOF synthesized using hydrofluoric acid as the modulator (13 and 12%, respectively; 4 and 5 percentage points). The hydrogen content found for the four MOFs nearly doubles the stoichiometric amount, with the largest deviation observed for the MOF synthesized using hydrofluoric acid as the modulator (2.2 percentage points). The sulfur content observed in Table 1 is 18–31% lower than the expected value, with the MOF synthesized using hydrofluoric acid again showing the highest deviation (3.1 percentage points). As shown in Table 1, minor amounts of nitrogen were also detected in every sample. Note that the sample with the highest nitrogen content, 4.4 wt.%, is precisely the one synthesized with hydrofluoric acid, the only sample that was not washed with DMF; therefore, the nitrogen content must come from the chromium nitrate salt used in all the syntheses. According to the elemental analysis results, the washing procedure involving hot water, DMF, and acetone proved better at removing unreacted products from the synthesized MOFs than just cold water and methanol. Overall, the elemental composition of the four samples is in good agreement with the stoichiometric composition of MIL-101(Cr)-SO₃H and with experimental data previously reported for MIL-101(Cr)-SO₃H [30]. The average deviation of the elemental analysis shown in Table 1 from the stoichiometric composition follows the order: hydrofluoric acid (23%) > acetic acid (18%) > without any modulator (16%) > nitric acid (15%).

Table 1. Elemental analysis and yield obtained of the MIL-101(Cr)-SO₃H samples synthesized without any modulator and using either hydrofluoric acid, acetic acid, or nitric acid as the modulator.

Modulator	Elemental Analysis (%, Mass, Dry Basis)					Yield (%, Mass)
	C	H	N	O	S	
-	28.7	3.3	0.8	44.0	8.0	32.6
Nitric acid	26.8	3.3	1.1	43.6	8.3	25.2
Acetic acid	30.3	3.5	2.1	43.2	7.9	29.6
Hydrofluoric acid	34.1	4.0	4.4	36.7	7.0	2.2

Table 1 also displays the yield of the MIL-101(Cr)-SO₃H syntheses, calculated based on the ligand. As observed, the highest yield was achieved in the absence of the modulator, followed by the synthesis employing acetic acid as the modulator, and then by that with nitric acid. It is noteworthy that the synthesis conducted using hydrofluoric acid as the modulator yielded a drastically lower yield.

Figure 1 shows the FTIR-ATR spectra of the MIL-101(Cr)-SO₃H samples synthesized without a modulator and using either hydrofluoric acid, acetic acid, or nitric acid as the modulator. The FTIR-ATR spectra of the four samples are in good agreement with the IR bands reported in the existing literature for MIL-101(Cr)-SO₃H [24,31]. Figure 1b shows the expected peaks at 1490 and 1404 cm⁻¹, which correspond to the symmetric and asymmetric coupling peaks of the carboxyl group (–O–C–O), respectively [27]. The bands shown in Figure 1b at 1228 and 1175 cm⁻¹ are attributed to the asymmetric and symmetric stretching vibrations of the O=S=O group, respectively [11,32,33], while the peak at 1078 cm⁻¹ is assigned to the in-plane skeletal vibration of the SO₃ group substituted on the aromatic rings of the terephthalate organic linker [34], and the band at 1023 cm⁻¹ is assigned to the S–O stretching vibration [35,36]. The peaks at 769 and 669 cm⁻¹ are ascribed to the C–S stretching vibration [37]. Other peaks corresponding to the sulfonic acid groups are also observed within the spectral region of 600 to 1400 cm⁻¹ [37,38]. The peaks at 543, 598 and

619 cm^{-1} can be attributed to the Cr–O stretching vibration [39,40]. No vibration at around the 1670 cm^{-1} wave number can be seen in Figure 1, indicating the absence of any residual ligand within the porous structure of the MOFs. The band at 1633 cm^{-1} is related to the presence of adsorbed water within the MOF structure [41]. Figure 1a shows a shoulder at 3170 cm^{-1} that is assigned to the –OH present in –SO₃H [42] within the broad band in the 3400 cm^{-1} region, characteristic of the –OH groups. It is noteworthy to highlight that the spectra of the four samples show the above-mentioned IR bands at similar wave numbers (the locations of the peak maxima differ by less than 4 cm^{-1}).

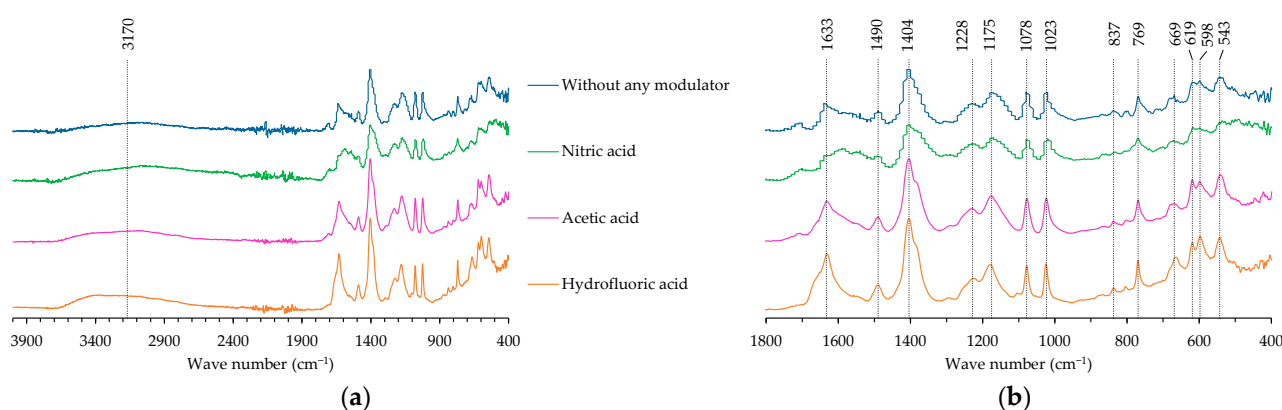


Figure 1. FTIR-ATR spectra of the MIL-101(Cr)-SO₃H samples synthesized without any modulator and using either hydrofluoric acid, acetic acid, or nitric acid as the modulator: (a) full spectra; (b) detail of the spectra in the $400\text{--}1800\text{ cm}^{-1}$ range.

Figure 2 shows the SEM micrographs of the MIL-101(Cr)-SO₃H samples synthesized without any modulator and using either hydrofluoric acid, acetic acid, or nitric acid as the modulator at 10,000 augmentations. Figure 2a shows the corresponding micrograph of the sample synthesized in the absence of a modulator: this presents the most heterogeneous morphology, exhibiting a mixture of spherical, planar and angulated particles of varying sizes. Shi and co-workers [33] reported that the diversity in crystal sizes could be ascribed to the drawbacks of the hydrothermal synthesis process. Figure 2b shows the micrograph of the sample synthesized using nitric acid as the modulator: despite the presence of some agglomerates in the background, the topology and particle size observed are much more uniform compared to Figure 2a. Figure 2c shows the micrograph of the sample synthesized using acetic acid as the modulator: the topology observed is more homogeneous and the particle size smaller than that of figures b and c. Figure 2d corresponds to the micrograph of the sample synthesized using hydrofluoric acid as the modulator: this exhibits the most homogeneous morphology of the series. The largest crystal size observed in Figure 2d entails the visualization of octahedra at only 10,000 augmentations. Octahedral crystals were visualized at higher augmentations within the SEM exploration of all samples, although the capture of high-resolution images of such octahedra was not possible due to the disintegration, distortion, movement and/or shrinkage of the same, which occurs as consequence of its non-conductive nature. The octahedral morphology of MIL-101(Cr)-SO₃H is consistent with the existing literature [33,43,44]. It is important to highlight the absence of needle-shaped crystals in the images, depicting the complete elimination of the ligand through the post-synthesis purification procedure [41,45].

Figure 3 represents the PXRD patterns of the MIL-101(Cr)-SO₃H samples synthesized without any modulator and using either hydrofluoric acid, acetic acid or nitric acid as the modulator. All the patterns are in good accordance with previous studies on MIL-101(Cr)-SO₃H [36,46–48] with slight differences in the position and relative intensities of the peaks among the patterns, thus confirming the successful synthesis and structural integrity of the four MOFs synthesized in this work. The PXRD patterns of all samples show the main characteristic diffraction peaks of MIL-101(Cr)-SO₃H at $2.9, 3.4, 4.1, 5.3$ and 9.2° , attributed

to the reflection planes of (220), (311), (400), (511) and (911), respectively [49]. The four samples also exhibit the characteristic diffraction peaks of MIL-101(Cr) at 5–9.5° [36,50]. The negligible peaks in the region $2\theta = 16\text{--}20^\circ$ affirm the successful removal of unreacted ligand crystals from the sample's framework [45]. The PXRD pattern of the sample synthesized with hydrofluoric acid possesses the narrowest peaks of the series, which is consistent with the larger crystal size observed in Figure 2d. The elevated background noise observed might be attributed to the irregular arrangement of $-\text{SO}_3^-$ groups and the substantial Compton-modified scattering originating from organic bridges within MIL-101(Cr)- SO_3H [27]. These bridges consist of numerous lightweight atoms such as carbon, oxygen, and hydrogen [49].

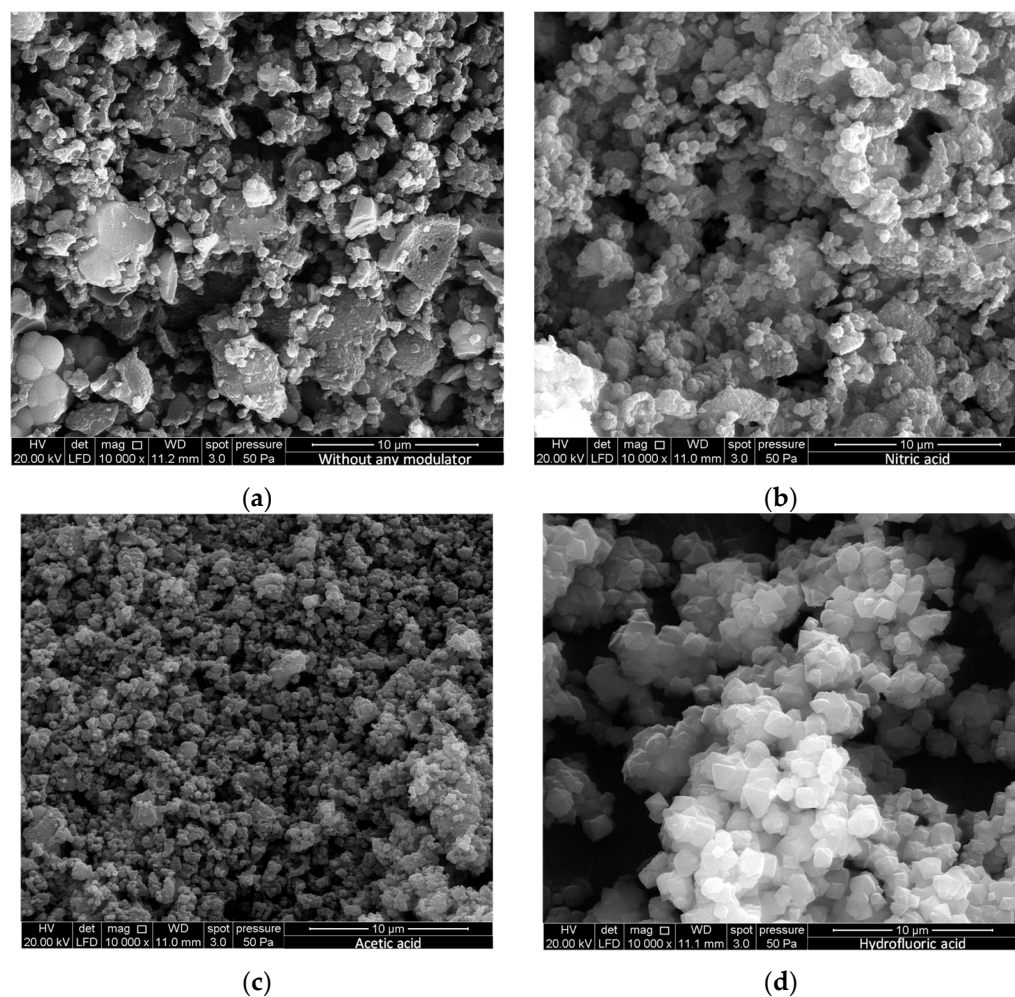


Figure 2. SEM images of MIL-101(Cr)- SO_3H samples synthesized without any modulator (a) and using either nitric acid (b), acetic acid (c), or hydrofluoric acid (d) as the modulator.

Figure 4 shows the TG curves and the weight loss of the MIL-101(Cr)- SO_3H samples synthesized without any modulator and using either hydrofluoric acid, acetic acid, or nitric acid as the modulator. Three main stages of mass loss can be distinguished, which are quantified in Table 2. The first stage of mass loss, with maxima between 77 and 103 °C, corresponds to the desolvation of the framework: the evaporation of solvent molecules within the pores and removal of water molecules. As can be seen in Table 2, the mass loss observed at this stage was significantly greater for the sample prepared using hydrofluoric acid as the modulator, which presented a mass loss of 27 wt.% below 200 °C. This might be attributed to the fact that this sample was washed making use of a less efficient washing procedure. The second stage of mass loss, which occurs in the temperature range between 200 and 400 °C, has a closer magnitude for all samples (11–16%). This is attributed to the thermal decomposition of the sulfonic acid moiety [51]. The third stage of mass loss, which

occurs above 400 °C, corresponds to the departure of the remaining OH⁻ ions, detachment of the organic linker, followed by the decomposition of the entire framework. This presents its maxima at ca. 540 °C. In this stage, the sample synthesized making use of acetic acid as the modulator exhibited the highest mass loss, 52 wt.%, whereas the sample synthesized with hydrofluoric acid presented the lowest mass loss, 30 wt.%. Overall, these results closely align with previous reports for MIL-101(Cr)-SO₃H [23,37,52].

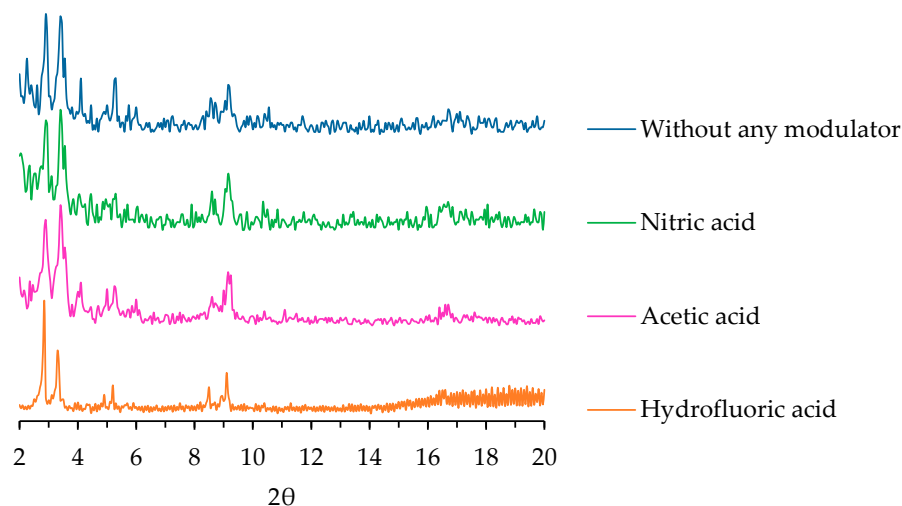


Figure 3. PXRD patterns of the MIL-101(Cr)-SO₃H samples synthesized without any modulator and using either hydrofluoric acid, acetic acid or nitric acid as the modulator.

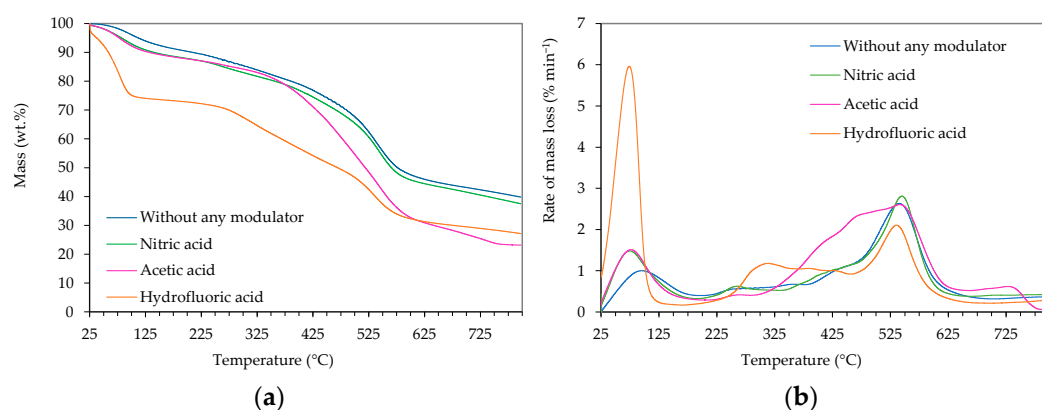


Figure 4. Thermogravimetric analysis of the MIL-101(Cr)-SO₃H samples synthesized without any modulator and using either hydrofluoric acid, acetic acid, or nitric acid as the modulator, using a heating rate of 10 °C min⁻¹ under N₂ flow: (a) mass evolution against temperature; (b) rate of mass loss observed versus temperature.

Table 2. Mass loss experienced by the MIL-101(Cr)-SO₃H samples during heating at 10 °C min⁻¹ under N₂ flow.

Temperature Range (°C)	Mass Loss (%)			
	Without Modulator	Nitric Acid	Acetic Acid	Hydrofluoric Acid
25–200	10	12	12	27
200–400	11	11	12	16
400–800	39	39	52	30

Figure 5 shows the N₂ adsorption isotherms at −196 °C of the MIL-101(Cr)-SO₃H samples synthesized without any modulator and using either hydrofluoric acid, acetic

acid, or nitric acid as the modulator. The filled symbols correspond to the adsorption data and the empty symbols to the desorption data. The adsorption isotherms show a type IVb topology, according to the updated classification proposed by the IUPAC [28] with completely reversible adsorption and desorption, characteristic of materials with narrow mesopores or cylindrical tapered end mesopores. All the isotherms shown in Figure 5 show five distinct zones: (i) a nearly vertical N_2 uptake is observed in the lowest-relative-pressure region corresponding to the filling of the narrowest micropores; (ii) then a somewhat less steep increase in the amount of N_2 adsorbed up to relative pressures of ca. 0.1; (iii) followed by a stage with an even softer slope; (iv) then a second steep zone ending at a relative pressure in the 0.2–0.3 range, with the actual ending point depending on the sample: 0.23 for the sample synthesized without any modulator, 0.30 for the sample synthesized using nitric acid as the modulator, 0.25 for the sample synthesized using acetic acid as the modulator, and 0.20 for the sample synthesized using hydrofluoric acid as the modulator; (v) the final stage consists of a gradual but moderate uptake that nearly resembles a plateau compared to the previous stages, which ends with a somewhat steeper slope at relative pressures close to unity. The overall isotherm topology resembles two consecutive steps that correspond to the filling of the micropores and the mesopores, respectively, which is consistent with the literature on MIL-101(Cr)- SO_3H [12,22,34,46].

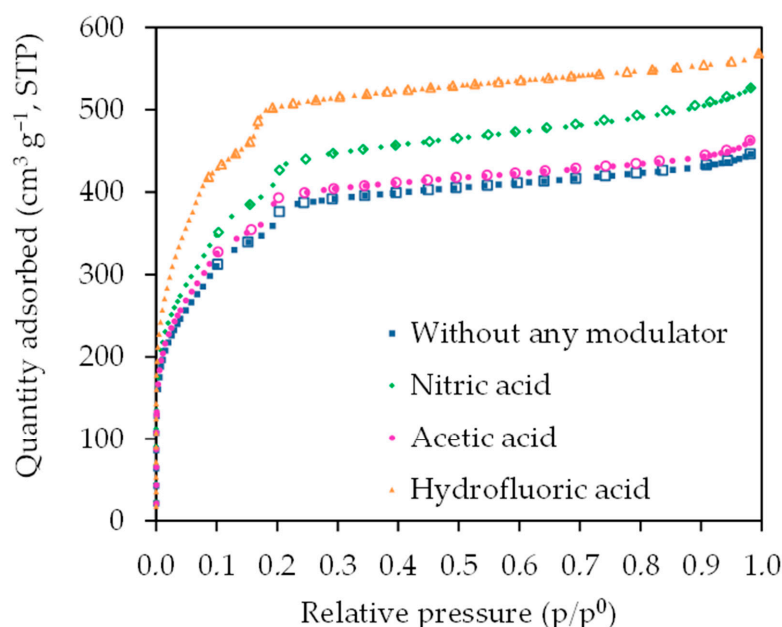


Figure 5. N_2 adsorption isotherms at $-196\text{ }^\circ\text{C}$ of the MIL-101(Cr)- SO_3H samples synthesized without any modulator and using either hydrofluoric acid, acetic acid, or nitric acid as the modulator. Full symbols represent adsorption data and empty symbols desorption data.

Table 3 presents the BET surface area, S_{BET} , and the total pore volume of the MIL-101(Cr)- SO_3H samples synthesized without any modulator and using either hydrofluoric acid, acetic acid, or nitric acid as modulators, together with previously reported values for MIL-101(Cr)- SO_3H , for comparison purposes.

The BET surface area of the MIL-101(Cr)- SO_3H MOFs synthesized in this work follows the order: hydrofluoric acid > nitric acid > acetic acid > without a modulator.

Table 3 shows that the BET surface area previously reported for the MIL-101(Cr)- SO_3H , synthesized making use of hydrofluoric acid as the modulator, ranges from 1066 to $2362\text{ m}^2\text{ g}^{-1}$ even under identical synthetic conditions (standard deviation: $439\text{ m}^2\text{ g}^{-1}$). The BET surface area of the MOF synthesized in this work making use of hydrofluoric acid, $1862\text{ m}^2\text{ g}^{-1}$, is above the average of those previously reported in the literature and summarized in Table 2: $1748\text{ m}^2\text{ g}^{-1}$.

Table 3. BET surface area and total pore volume of the MIL-101(Cr)-SO₃H samples synthesized in this work without any modulator and using either hydrofluoric acid, acetic acid, or nitric acid as the modulator, and of other MIL-101(Cr)-SO₃H samples reported in the literature.

Modulator	S _{BET} (m ² g ⁻¹)	Total Pore Volume (cm ³ g ⁻¹)	Reference
-	1342	0.69	This work
Nitric acid	1554	0.81	This work
Acetic acid	1374	0.72	This work
Hydrofluoric acid	1862	0.87	This work
Hydrofluoric acid	1800	-	[24]
Hydrofluoric acid	1501	-	[35]
Hydrofluoric acid	1066	-	[36]
Hydrofluoric acid	2362	1.33	[44]
Hydrofluoric acid	1754	-	[47]
Hydrofluoric acid	1550	1.3	[48]
Hydrofluoric acid	2206	1.27	[51]
Hydrochloric acid	1937	-	[11]
Hydrochloric acid	1200	-	[24]
Hydrochloric acid	1915	-	[26]
Hydrochloric acid	334	-	[27]
Hydrochloric acid	1706	1.01	[33]
Hydrochloric acid	1603	-	[34]
Hydrochloric acid	1362	-	[35]
Hydrochloric acid	1497	-	[37]
Hydrochloric acid	1599	-	[46]
Hydrochloric acid	1937	-	[50]
Sodium acetate	1115	-	[12]
Sodium acetate	1376	-	[35]

The average value of the BET surface areas previously reported for the MIL-101(Cr)-SO₃H samples synthesized making use of sodium acetate as the modulator, $1246 \pm 185 \text{ m}^2 \text{ g}^{-1}$, is below those obtained in this work. On the other hand, looking at the average value of the BET surface areas previously reported for the MIL-101(Cr)-SO₃H samples synthesized making use of hydrochloric acid as the modulator, $1494 \pm 508 \text{ m}^2 \text{ g}^{-1}$, one might conclude that hydrochloric acid is a better modulator than nitric and acetic acid. However, it is important to highlight that comparisons are not straightforward, as other synthetic conditions also change. For example, all the synthetic routes that involve the use of hydrochloric acid as the modulator summarized in Table 3 make use of longer reaction times than that used in this work (24 h): Lee and Pien heated the reaction mixture for 5 days at the higher temperature of 240 °C [27]; Wang et al. [50] and Xie et al. [11] heated the reaction mixture at 180 °C for 3 days. Several authors heated the reaction mixture at 180 °C for 6 days [26,33–35,46], Devarajan and Suresh [37], and Juan-Alcañiz et al. [24], heated the reaction mixture at 180 °C for 7 days. Saikia and Saikia used a post-synthetic modification method to sulfonate the MIL-101(Cr) framework using chlorosulfonic acid in dichloromethane [51].

The BET surface area shown in Table 3 for the MIL-101(Cr)-SO₃H samples synthesized in this work using acetic acid as the modulator is similar to the value reported by Ma et al. using sodium acetate [35], under otherwise comparable synthetic conditions, and slightly above that of hydrochloric acid [24,35]. This is higher than the value reported by Li et al. using hydrofluoric acid [36], the value reported by Lee and Pien [27], as well as Juan-Alcañiz et al. [24], using hydrochloric acid, and the value reported by Ramsperger et al. [12] making use of sodium acetate as the modulator.

The total pore volume of the MIL-101(Cr)-SO₃H MOFs synthesized in this work follows the order: hydrofluoric acid > nitric acid > acetic acid > without any modulator. As can be seen in Table 3, the values obtained in this research are lower than the ones reported in the literature [33,44,48,51].

Figure 6 represents the PSD of the MIL-101(Cr)-SO₃H samples synthesized without any modulator and using either hydrofluoric acid, acetic acid, or nitric acid as the modulator. Figure 6 shows a bimodal distribution with maxima at 6 Å and at 20 Å for the sample synthesized with hydrofluoric acid, 6 Å and at 22 Å for the sample synthesized with acetic acid, 7 Å and at 22 Å for the sample synthesized with nitric acid, and at 6 and 22 Å for the sample synthesized without any modulator. These bimodal PSD can be ascribed to the pentagonal windows with 5–12 Å pore width and the pentagonal–hexagonal windows with 12–20 Å pore width of MIL-101(Cr) [31,45]. Previously published PSDs for MIL-101(Cr)-SO₃H only show the range 10–100 Å, with pores with a width of 10–20 Å [35] or 10–30 Å [46,47].

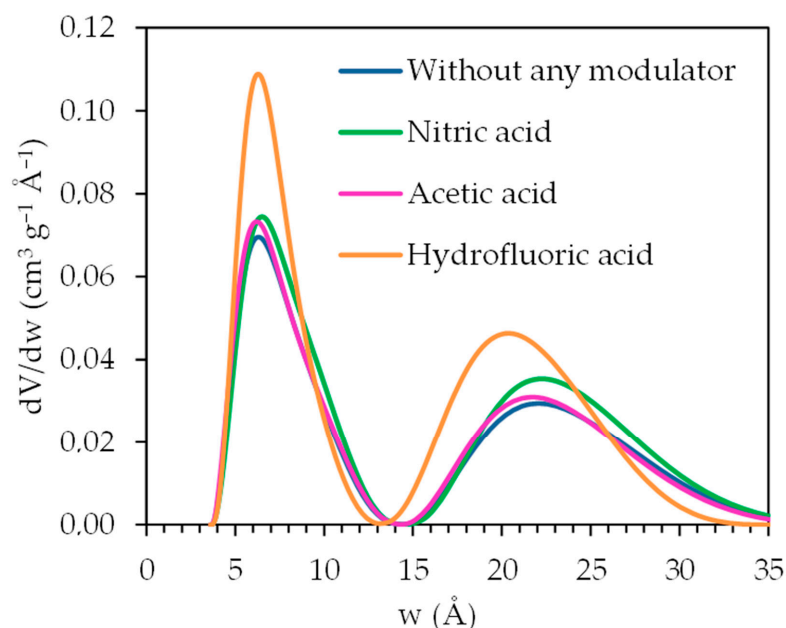


Figure 6. PSD of the MIL-101(Cr)-SO₃H samples synthesized without any modulator and using either hydrofluoric acid, acetic acid or nitric acid as the modulator.

3.2. The Effect of the Dose of Acetic Acid on the Synthesis of MIL-101(Cr)-SO₃H

In Section 3.1, the same volume of modulator, 0.3 mL, was used in all cases for comparison purposes. However, this corresponded to 8 mmol of hydrofluoric acid [22], but ca. 5 mmol of nitric acid and acetic acid. In an attempt to improve the textural properties of the hydrofluoric acid-free samples, the effect of the dose of acetic acid added to the reaction mixture was investigated: four additional syntheses were conducted using 4, 8, 10 and 15 mmol of acetic acid, following the synthetic protocol described in Section 2.2.

Table 4 shows the elemental analysis for the MIL-101(Cr)-SO₃H series synthesized with increasing doses of acetic acid. As observed in the table, the carbon and oxygen contents match the theoretical values across all samples (average deviations of 1% and 2%, respectively; 0.2–2 and 0.4–2.3 percentage points). On the other hand, the hydrogen content of the series nearly doubles the stoichiometric value. The sulfur content is only somewhat lower than expected (20% on average; 2.1 percentage points). As shown in Table 4, minor amounts of nitrogen were detected in every sample. As discussed in Section 3.1, this is attributed to the chromium nitrate salt. In general, the elemental composition of the series was found to be in good agreement with the stoichiometric composition of MIL-101(Cr)-SO₃H, confirming the successful formation of the framework.

Table 4 also displays the yield of the MIL-101(Cr)-SO₃H syntheses, calculated based on the ligand. As observed, the mass yield decreases when the amount of acetic acid incorporated in the reaction mixture increases. A similar behavior was found by Zhao et al. when they synthesized MIL-101(Cr) using acetic acid as the modulator [25].

Table 4. Elemental analysis and yield obtained of the MIL-101(Cr)-SO₃H series synthesized with increasing doses of acetic acid.

Acetic Acid Dose (mmol)	Elemental Analysis (% Mass, Dry Basis)					Yield (%, Mass)
	C	H	N	O	S	
4	31.0	3.5	2.3	41.3	7.5	37.0
5	30.3	3.5	2.1	43.2	7.9	29.6
8	29.7	3.7	2.1	42.2	8.1	28.9
10	28.1	3.5	1.0	44.1	8.5	27.8
15	29.7	3.4	1.2	42.4	8.2	25.9

Figure 7 shows the FTIR-ATR spectra of the MIL-101(Cr)-SO₃H samples synthesized with increasing doses of acetic acid. The FTIR spectra of these five samples are similar, with the corresponding peak maxima differing by less than 4 cm⁻¹. These spectra are alike to those described in Section 3.1, confirming the formation of MIL-101(Cr)-SO₃H. The positions of the peaks in Figure 7 only exhibit slight variations compared to those of Figure 1. Briefly, the bands corresponding to the symmetric and asymmetric coupling peaks of the carboxyl group (–O–C–O) are at 1489 and 1404 cm⁻¹, respectively. The peaks attributed to the asymmetric and symmetric stretching vibrations of the O=S=O group appear at 1225 and 1175 cm⁻¹, respectively. The peak corresponding to the in-plane skeletal vibration of the SO₃ group substituted on the aromatic rings of the terephthalate organic linker appears at 1077 cm⁻¹, and the band corresponding to the S–O stretching vibration is present at 1024 cm⁻¹. The peaks attributed to the C–S stretching vibration appear at the same wave numbers as reported in Section 3.1, 769 and 669 cm⁻¹. Additionally, peaks corresponding to sulfonic acid groups are also observed within the spectral range of 600 to 1400 cm⁻¹. The peaks attributed to the Cr–O stretching vibration are present at 541, 597 and 618 cm⁻¹. Regarding the broad region characteristic of the –OH groups, the shoulder at 3120 cm⁻¹ is assigned to the –OH present in –SO₃H. The band associated with the presence of adsorbed water within the MOF structure appears at 1627 cm⁻¹. As mentioned in Section 3.1, no vibration was detected at ca. 1670 cm⁻¹ (seen in Figure 7), suggesting the absence of any residual ligand within the porous structure of the MOFs.

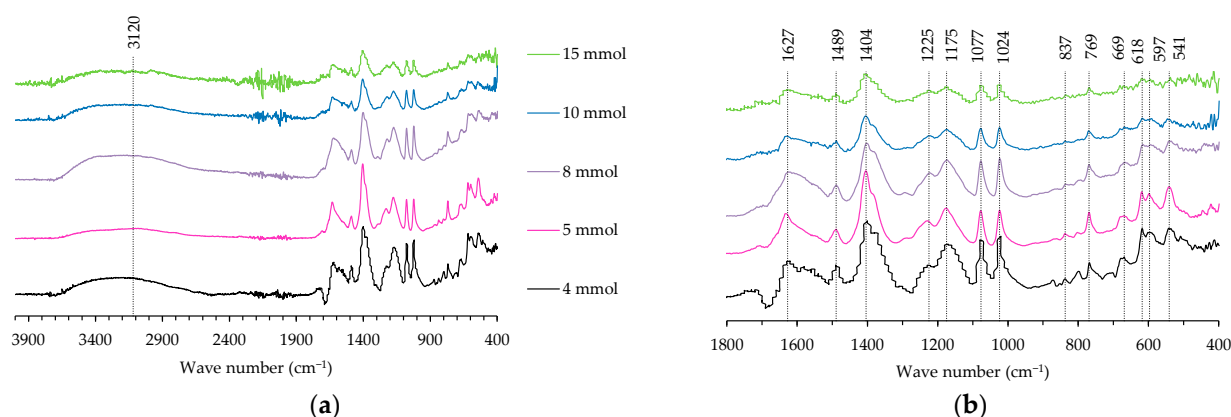
**Figure 7.** FTIR-ATR spectra of the MIL-101(Cr)-SO₃H samples synthesized with increasing doses of acetic acid: (a) full spectra; (b) detail of the spectra in the 400–1800 cm⁻¹ range.

Figure 8 shows the PXRD patterns of the MIL-101(Cr)-SO₃H samples synthesized with increasing doses of acetic acid. The patterns of all samples present the expected diffraction peaks, described in Section 3.1, with minor variations in the position of the peaks. Therefore, they confirm the successful synthesis and structural integrity of the five samples.

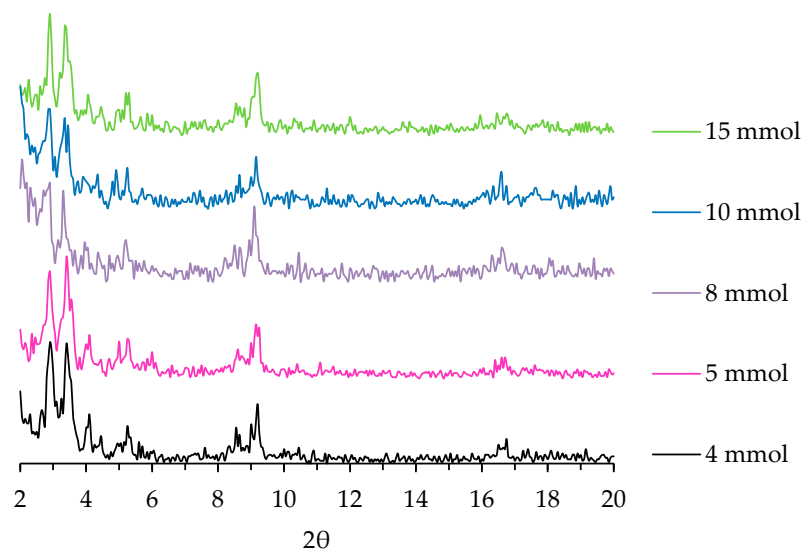


Figure 8. PXRD patterns of the MIL-101(Cr)-SO₃H samples synthesized with increasing doses of acetic acid.

Figure 9 shows the N₂ adsorption isotherms at −196 °C of the MIL-101(Cr)-SO₃H samples synthesized with increasing doses of acetic acid. These have a similar topology to those already shown in Figure 5 (type IVb), resembling two consecutive steps corresponding to the filling of the micropores and the mesopores, respectively.

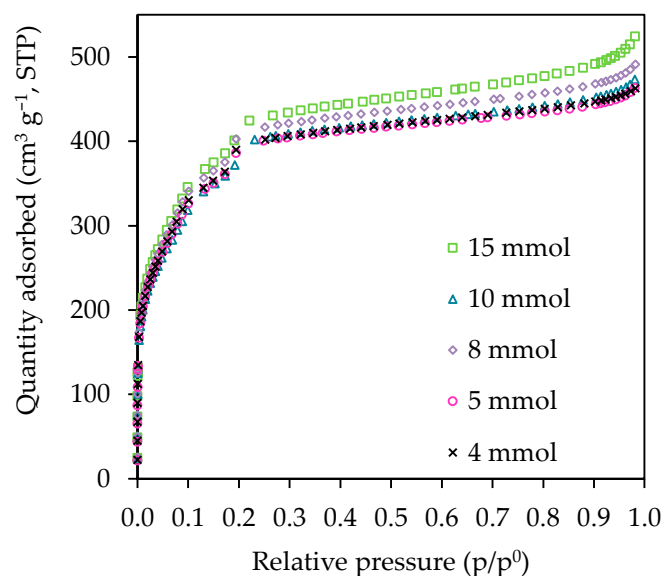


Figure 9. N₂ adsorption isotherms at −196 °C of the MIL-101(Cr)-SO₃H samples synthesized with increasing doses of acetic acid.

Table 5 presents the BET surface area and the total pore volume of the MIL-101(Cr)-SO₃H samples synthesized with increasing amounts of acetic acid. In general, the BET surface area and the total pore volume both exhibit an increase with the dose of the acetic acid added in the synthesis of MIL-101(Cr)-SO₃H, except for the sample synthesized using a dose of 10 mmol of acetic acid, which shows slightly lower BET surface area and pore volume compared to the sample synthesized by adding 8 mmol of acetic acid.

The molar ratio of nitric acid to chromium salt used in Section 3.1 was 0.9, and the molar ratio of nitric acid to ligand was 0.5. Previous investigations on the search for a hydrofluoric acid-free synthesis method of the parent MOF, MIL-101(Cr), have found that employing a 1:1:1 ratio of nitric acid to chromium and to ligand yields the highest BET

surface area, $3450 \text{ m}^2 \text{ g}^{-1}$, but that deviating from this ratio, either by excess or deficit, results in a decrease in surface area [25]. Alivand et al. explored the impact of nitric acid and its optimal dosage in the formation reaction by varying nitric acid-to-ligand ratios of 0.5, 1, and 2. Remarkably, the equimolar sample exhibited the highest BET surface area and pore volume, reaching $3841 \text{ m}^2 \text{ g}^{-1}$ and $1.72 \text{ cm}^3 \text{ g}^{-1}$, respectively. These values exceeded those obtained using hydrofluoric acid as a modulator, which recorded a BET surface area of $3609 \text{ m}^2 \text{ g}^{-1}$ and a pore volume of $1.55 \text{ cm}^3 \text{ g}^{-1}$ [45].

Table 5. BET surface area, micropore volume and total pore volume of the MIL-101(Cr)-SO₃H samples synthesized with increasing doses of acetic acid, and molar ratio of acetic acid added to salt and ligand.

mmol of Acetic Acid Added	S_{BET} ($\text{m}^2 \text{ g}^{-1}$)	Total Pore Volume ($\text{cm}^3 \text{ g}^{-1}$)	Molar Ratio of Acetic Acid to Salt	Molar Ratio of Acetic Acid to Ligand
4	1374	0.71	0.8	0.4
5	1374	0.72	1.05	0.525
8	1427	0.76	1.6	0.8
10	1407	0.73	2	1
15	1504	0.81	3	1.5

Acetic acid has also been proposed as a modulator for the synthesis of the parent MOF, MIL-101(Cr). In the work of Zhao et al., the best outcome was achieved for a ratio of acetic acid to Cr and ligand of 8.3:1:1, yielding a BET surface area of $2750 \text{ m}^2 \text{ g}^{-1}$; surpassing this quantity led to the absence of isolated products [25]. In the present study, the highest BET surface area was achieved for the highest dose of acetic acid investigated, which corresponds to a molar ratio of 3 to the chromium salt and 1.5 to the ligand, as can be seen in Table 5. Rallapalli et al. demonstrated that using a 1:1 ratio of acetic acid to chromium salt in the synthesis of MIL-101(Cr) yielded a higher BET surface area of $3326 \text{ m}^2 \text{ g}^{-1}$ compared to the original hydrofluoric acid-based protocol, which yielded $2887 \text{ m}^2 \text{ g}^{-1}$ [42]. However, in the present investigation, employing a nearly equimolar ratio of modulator to ligand, which corresponds to the syntheses utilizing 4 and 5 mmol of acetic acid, as can be seen in Table 5, yielded the lowest BET surface area and total pore volume of the series.

Figure 10 represents the PSD of the MIL-101(Cr)-SO₃H samples synthesized with varying amounts of acetic acid. A bimodal PSD with maxima at 6 Å and 22 Å is observed for all the samples, except for the sample synthesized using 10 mmol of acetic acid, which presents the second maxima slightly displaced to 23 Å. This bimodal PSD is attributed to the pentagonal windows with 5–12 Å pore width and pentagonal–hexagonal windows with 12–20 Å pore width of MIL-101(Cr), as already discussed in Section 3.1.

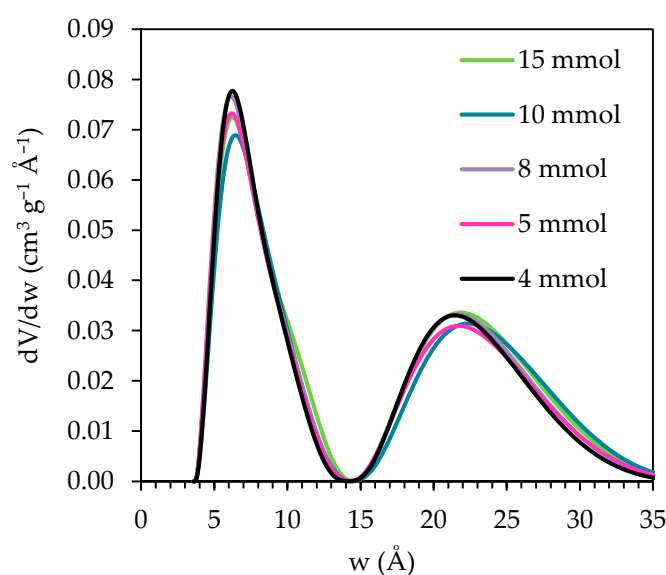


Figure 10. PSD of the MIL-101(Cr)-SO₃H samples synthesized with increasing doses of acetic acid.

4. Conclusions

In this research, acetic and nitric acids were evaluated as alternative modulators to hydrofluoric acid in the synthesis of MIL-101(Cr)-SO₃H. The utilization of acetic and nitric acids as modulators not only proved to be a viable, environmentally friendlier, and safer alternative to the use of hydrofluoric acid but was also shown to provide significantly higher yields of MIL-101(Cr)-SO₃H.

The synthesis of MIL-101(Cr)-SO₃H by making use of acetic acid as the modulator proved able to provide a superior synthetic yield and purity than those accomplished with nitric acid and much more superior than those when using hydrofluoric acid.

The BET surface area and the total pore volume of the syntheses accomplished using the different modulators evaluated followed the order: hydrofluoric acid > nitric acid > acetic acid > without a modulator.

The dose of acetic acid was investigated, and it was found that increasing the amount of acetic acid from 4 to 15 mmol led to an increase in the BET surface area, from 1374 to 1504 m² g⁻¹, and of the total pore volume, from 0.71 to 0.81, at the expense of a reduction in the yield of MIL 101(Cr)-SO₃H from 37.0 to 25.9 wt.%.

The yield of MIL 101(Cr)-SO₃H obtained using the highest acetic acid molar ratio to salt and ligand evaluated, 3 and 1.5, respectively, was 12 times higher than that obtained with hydrofluoric acid, at the expense of a moderate reduction in the BET surface area of only 19%.

Author Contributions: Conceptualization, T.M.B. and M.G.P.; methodology, T.M.B. and M.G.P.; formal analysis, T.M.B. and M.G.P.; investigation, T.M.B.; resources, M.G.P. and F.R.; data curation, T.M.B. and M.G.P.; writing—original draft preparation, T.M.B.; writing—review and editing, M.G.P. and F.R.; visualization, T.M.B. and M.G.P.; supervision, M.G.P. and F.R.; project administration, M.G.P.; funding acquisition, T.M.B., M.G.P. and F.R. All authors have read and agreed to the published version of the manuscript.

Funding: T. M. Bernal acknowledges the financial support received from the Spanish Ministry of Universities for the Training of University Lecturers (FPU pre-doctoral aid program FPU21/02425).

Data Availability Statement: Data are contained within the article.

Conflicts of Interest: The authors declare no conflicts of interest.

References

1. Rico-Barragán, A.A.; Álvarez, J.R.; Hernández-Fernández, E.; Rodríguez-Hernández, J.; Garza-Navarro, M.A.; Dávila-Guzmán, N.E. Green Synthesis of Metal-Organic Framework MIL-101(Cr)—An Assessment by Quantitative Green Chemistry Metrics. *Polyhedron* **2022**, *225*, 116052. [[CrossRef](#)]
2. Zorainy, M.Y.; Gar Alalm, M.; Kaliaguine, S.; Boffito, D.C. Revisiting the MIL-101 Metal-Organic Framework: Design, Synthesis, Modifications, Advances, and Recent Applications. *J. Mater. Chem. A Mater.* **2021**, *9*, 22159–22217. [[CrossRef](#)]
3. Darunte, L.A.; Oetomo, A.D.; Walton, K.S.; Sholl, D.S.; Jones, C.W. Direct Air Capture of CO₂ Using Amine Functionalized MIL-101(Cr). *ACS Sustain. Chem. Eng.* **2016**, *4*, 5761–5768. [[CrossRef](#)]
4. Giles-Mazón, E.A.; Germán-Ramos, I.; Romero-Romero, F.; Reinheimer, E.; Toscano, R.A.; Lopez, N.; Barrera-Díaz, C.E.; Varela-Guerrero, V.; Ballesteros-Rivas, M.F. Synthesis and Characterization of a Bio-MOF Based on Mixed Adeninate/Tricarboxylate Ligands and Zinc Ions. *Inorganica. Chim. Acta* **2018**, *469*, 306–311. [[CrossRef](#)]
5. Zou, M.; Dong, M.; Zhao, T. Advances in Metal-Organic Frameworks MIL-101(Cr). *Int. J. Mol. Sci.* **2022**, *23*, 9396. [[CrossRef](#)] [[PubMed](#)]
6. Seetharaj, R.; Vandana, P.V.; Arya, P.; Mathew, S. Dependence of Solvents, PH, Molar Ratio and Temperature in Tuning Metal Organic Framework Architecture. *Arab. J. Chem.* **2019**, *12*, 295–315. [[CrossRef](#)]
7. Bhattacharjee, S.; Chen, C.; Ahn, W.S. Chromium Terephthalate Metal-Organic Framework MIL-101: Synthesis, Functionalization, and Applications for Adsorption and Catalysis. *RSC Adv.* **2014**, *4*, 52500–52525. [[CrossRef](#)]
8. Zhong, R.; Yu, X.; Meng, W.; Liu, J.; Zhi, C.; Zou, R. Amine-Grafted MIL-101(Cr) via Double-Solvent Incorporation for Synergistic Enhancement of CO₂ Uptake and Selectivity. *ACS Sustain. Chem. Eng.* **2018**, *6*, 16493–16502. [[CrossRef](#)]
9. Nie, J.; Pang, Y.; Liu, J.; Kong, X.; Zhang, H. Experimental Investigation on Air Dehumidification Performance of Metal Organic Frameworks and Its Application Potential for Solid Desiccant Air Conditioning Systems. *Sci. Technol. Built. Environ.* **2023**, *29*, 230–240. [[CrossRef](#)]

10. Gordeeva, L.G.; Solovyeva, M.V.; Sapienza, A.; Aristov, Y.I. Potable Water Extraction from the Atmosphere: Potential of MOFs. *Renew. Energy* **2020**, *148*, 72–80. [[CrossRef](#)]
11. Xie, Y.; Fang, Z.; Li, L.; Yang, H.; Liu, T.F. Creating Chemisorption Sites for Enhanced CO₂ Photoreduction Activity through Alkylamine Modification of MIL-101-Cr. *ACS Appl. Mater. Interfaces* **2019**, *11*, 27017–27023. [[CrossRef](#)] [[PubMed](#)]
12. Ramsperger, C.A.; Tufts, N.Q.; Yadav, A.K.; Lessard, J.M.; Stylianou, K.C. Sustainable and Chemoselective Synthesis of α -Aminonitriles Using Lewis and Brønsted Acid-Functionalized Nanoconfined Spaces. *ACS Appl. Mater. Interfaces* **2022**, *14*, 49957–49964. [[CrossRef](#)] [[PubMed](#)]
13. Chołuj, A.; Karczykowski, R.; Chmielewski, M.J. Simple and Robust Immobilization of a Ruthenium Olefin Metathesis Catalyst Inside MOFs by Acid-Base Reaction. *Organometallics* **2019**, *38*, 3392–3396. [[CrossRef](#)]
14. Liu, X.; Pan, H.; Zhang, H.; Li, H.; Yang, S. Efficient Catalytic Upgradation of Bio-Based Furfuryl Alcohol to Ethyl Levulinate Using Mesoporous Acidic MIL-101(Cr). *ACS Omega* **2019**, *4*, 8390–8399. [[CrossRef](#)] [[PubMed](#)]
15. Chaemchuen, S.; Xiao, X.; Klomklang, N.; Yusubov, M.S.; Verpoort, F. Tunable Metal–Organic Frameworks for Heat Transformation Applications. *Nanomaterials* **2018**, *8*, 661. [[CrossRef](#)] [[PubMed](#)]
16. Steinert, D.M.; Ernst, S.J.; Henninger, S.K.; Janiak, C. Metal–Organic Frameworks as Sorption Materials for Heat Transformation Processes. *Eur. J. Inorg. Chem.* **2020**, *2020*, 4502–4515. [[CrossRef](#)]
17. Rim, G.; Kong, F.; Song, M.; Rosu, C.; Priyadarshini, P.; Lively, R.P.; Jones, C.W. Sub-Ambient Temperature Direct Air Capture of CO₂ Using Amine-Impregnated MIL-101(Cr) Enables Ambient Temperature CO₂ Recovery. *JACS Au* **2022**, *2*, 380–393. [[CrossRef](#)] [[PubMed](#)]
18. Dong, Y.; Xing, J.; Zhao, T.; Peng, S. In Situ Growth of MIL-101(Cr)-SO₃H Sphere on Polyethylenimine-Reduced Graphene Oxide and Its Application as Dopamine Sensor. *Diam. Relat. Mater.* **2023**, *139*, 110304. [[CrossRef](#)]
19. Dahiya, M.S.; Tomer, V.K.; Duhan, S. Metal-Ferrite Nanocomposites for Targeted Drug Delivery. In *Applications of Nanocomposite Materials in Drug Delivery*, 1st ed.; Enamuddin, A.M., Asiri, A.M., Eds.; Woodhead Publishing: Sawston, UK, 2018; pp. 737–760.
20. Sariga; Ayilliath Kolaprath, M.K.; Benny, L.; Varghese, A. A Facile, Green Synthesis of Carbon Quantum Dots from Polyalthia Longifolia and Its Application for the Selective Detection of Cadmium. *Dye. Pigment.* **2023**, *210*, 111048. [[CrossRef](#)]
21. Ghawade, S.P.; Pande, K.N.; Dhoble, S.J.; Deshmukh, A.D. Tuning the Properties of ZnS Semiconductor by the Addition of Graphene. In *Nanoscale Compound Semiconductors and Their Optoelectronics Applications*, 1st ed.; Pawade, V.B., Dhoble, S.J., Hendrik, C.S., Eds.; Woodhead Publishing: Sawston, UK, 2022; pp. 351–381.
22. Li, H.; Wang, K.; Feng, D.; Chen, Y.P.; Verdegaal, W.; Zhou, H.C. Incorporation of Alkylamine into Metal–Organic Frameworks through a Brønsted Acid–Base Reaction for CO₂ Capture. *ChemSusChem* **2016**, *9*, 2832–2840. [[CrossRef](#)]
23. Ren, X.; Wang, C.C.; Li, Y.; Wang, P.; Gao, S. Defective SO₃H-MIL-101(Cr) for Capturing Different Cationic Metal Ions: Performances and Mechanisms. *J. Hazard. Mater.* **2023**, *445*, 130552. [[CrossRef](#)]
24. Juan-Alcañiz, J.; Giellisse, R.; Lago, A.B.; Ramos-Fernandez, E.V.; Serra-Crespo, P.; Devic, T.; Guillou, N.; Serre, C.; Kapteijn, F.; Gascon, J. Towards Acid MOFs-Catalytic Performance of Sulfonic Acid Functionalized Architectures. *Catal. Sci. Technol.* **2013**, *3*, 2311–2318. [[CrossRef](#)]
25. Zhao, T.; Jeremias, F.; Boldog, I.; Nguyen, B.; Henninger, S.K.; Janiak, C. High-Yield, Fluoride-Free and Large-Scale Synthesis of MIL-101(Cr). *Dalton Trans.* **2015**, *44*, 16791–16801. [[CrossRef](#)] [[PubMed](#)]
26. Akiyama, G.; Matsuda, R.; Sato, H.; Takata, M.; Kitagawa, S. Cellulose Hydrolysis by a New Porous Coordination Polymer Decorated with Sulfonic Acid Functional Groups. *Adv. Mater.* **2011**, *23*, 3294–3297. [[CrossRef](#)] [[PubMed](#)]
27. Lee, K.T.; Pien, C.Y. Preparation of Monosodium 2-Sulfoterephthalate to Make a MIL-101(Cr)-SO₃H Catalyst. *New J. Chem.* **2022**, *46*, 868–876. [[CrossRef](#)]
28. Thommes, M.; Kaneko, K.; Neimark, A.V.; Olivier, J.P.; Rodriguez-Reinoso, F.; Rouquerol, J.; Sing, K.S.W. Physisorption of Gases, with Special Reference to the Evaluation of Surface Area and Pore Size Distribution (IUPAC Technical Report). *Pure Appl. Chem.* **2015**, *87*, 1051–1069. [[CrossRef](#)]
29. Rouquerol, J.; Llewellyn, P.; Rouquerol, F. Is the BET Equation Applicable to Microporous Adsorbents? *Stud. Surf. Sci. Catal.* **2007**, *160*, 49–56. [[CrossRef](#)]
30. Gkaniatsou, E.; Ricoux, R.; Kariyawasam, K.; Stenger, I.; Fan, B.; Ayoub, N.; Salas, S.; Patriarche, G.; Serre, C.; Mahy, J.P.; et al. Encapsulation of Microperoxidase-8 in MIL-101(Cr)-X Nanoparticles: Influence of Metal–Organic Framework Functionalization on Enzymatic Immobilization and Catalytic Activity. *ACS Appl. Nano Mater.* **2020**, *3*, 3233–3243. [[CrossRef](#)]
31. Santiago-Portillo, A.; Navalón, S.; Concepción, P.; Álvaro, M.; García, H. Influence of Terephthalic Acid Substituents on the Catalytic Activity of MIL-101(Cr) in Three Lewis Acid Catalyzed Reactions. *ChemCatChem* **2017**, *9*, 2506–2511. [[CrossRef](#)]
32. Mortazavi, S.S.; Abbasi, A.; Masteri-Farahani, M. Influence of -SO₃H Groups Incorporated as Brønsted Acidic Parts by Tandem Post-Synthetic Functionalization on the Catalytic Behavior of MIL-101(Cr) MOF for Methanolysis of Styrene Oxide. *Colloids Surf. A Physicochem. Eng. Asp.* **2020**, *599*, 124703. [[CrossRef](#)]
33. Shi, W.; Zhu, Y.; Shen, C.; Shi, J.; Xu, G.; Xiao, X.; Cao, R. Water Sorption Properties of Functionalized MIL-101(Cr)-X (X = -NH₂, -SO₃H, H, -CH₃, -F) Based Composites as Thermochemical Heat Storage Materials. *Microporous Mesoporous Mater.* **2019**, *285*, 129–136. [[CrossRef](#)]
34. Sun, W.J.; Gao, E.Q. Sulfonic-Functionalized MIL-101 as Bifunctional Catalyst for Cyclohexene Oxidation. *Mol. Catal.* **2020**, *482*, 110746. [[CrossRef](#)]

35. Ma, L.; Xu, L.; Jiang, H.; Yuan, X. Comparative Research on Three Types of MIL-101(Cr)-SO₃H for Esterification of Cyclohexene with Formic Acid. *RSC Adv.* **2019**, *9*, 5692–5700. [[CrossRef](#)] [[PubMed](#)]
36. Li, X.; Zhou, Z.; Zhao, Y.; Ramella, D.; Luan, Y. Copper-Doped Sulfonic Acid-Functionalized MIL-101(Cr) Metal–Organic Framework for Efficient Aerobic Oxidation Reactions. *Appl. Organomet. Chem.* **2020**, *34*, e5445. [[CrossRef](#)]
37. Devarajan, N.; Suresh, P. MIL-101-SO₃H Metal–Organic Framework as a Brønsted Acid Catalyst in Hantzsch Reaction: An Efficient and Sustainable Methodology for One-Pot Synthesis of 1,4-Dihydropyridine. *New J. Chem.* **2019**, *43*, 6806–6814. [[CrossRef](#)]
38. Hasan, Z.; Jun, J.W.; Jhung, S.H. Sulfonic Acid-Functionalized MIL-101(Cr): An Efficient Catalyst for Esterification of Oleic Acid and Vapor-Phase Dehydration of Butanol. *Chem. Eng. J.* **2015**, *278*, 265–271. [[CrossRef](#)]
39. Ivanova, T.; Gesheva, K.; Cziraki, A.; Szekeres, A.; Vlaikova, E. Structural Transformations and Their Relation to the Optoelectronic Properties of Chromium Oxide Thin Films. *J. Phys. Conf. Ser.* **2008**, *113*, 012030. [[CrossRef](#)]
40. Madi, C.; Tabbal, M.; Christidis, T.; Isber, S.; Nsouli, B.; Zahraman, K. Microstructural Characterization of Chromium Oxide Thin Films Grown by Remote Plasma Assisted Pulsed Laser Deposition. *J. Phys. Conf. Ser.* **2007**, *59*, 600–604. [[CrossRef](#)]
41. Shafiei, M.; Alivand, M.S.; Rashidi, A.; Samimi, A.; Mohebbi-Kalhari, D. Synthesis and Adsorption Performance of a Modified Micro-Mesoporous MIL-101(Cr) for VOCs Removal at Ambient Conditions. *Chem. Eng. J.* **2018**, *341*, 164–174. [[CrossRef](#)]
42. Rallapalli, P.B.S.; Raj, M.C.; Senthikumar, S.; Somani, R.S.; Bajaj, H.C. HF-Free Synthesis of MIL-101(Cr) and Its Hydrogen Adsorption Studies. *Environ. Prog. Sustain. Energy* **2016**, *35*, 461–468. [[CrossRef](#)]
43. Mortazavi, S.S.; Abbasi, A.; Masteri-Farahani, M.; Farzaneh, F. Sulfonic Acid Functionalized MIL-101(Cr) Metal–Organic Framework for Catalytic Production of Acetals. *ChemistrySelect* **2019**, *4*, 7495–7501. [[CrossRef](#)]
44. Chen, J.; Zhang, Y.; Chen, X.; Dai, S.; Bao, Z.; Yang, Q.; Ren, Q.; Zhang, Z. Cooperative Interplay of Brønsted Acid and Lewis Acid Sites in MIL-101(Cr) for Cross-Dehydrogenative Coupling of C–H Bonds. *ACS Appl. Mater. Interfaces* **2021**, *13*, 10845–10854. [[CrossRef](#)]
45. Sheikh Alivand, M.; Hossein Tehrani, N.H.M.; Shafiei-Alavijeh, M.; Rashidi, A.; Kooti, M.; Pourreza, A.; Fakhraie, S. Synthesis of a Modified HF-Free MIL-101(Cr) Nanoadsorbent with Enhanced H₂S/CH₄, CO₂/CH₄, and CO₂/N₂ Selectivity. *J. Environ. Chem. Eng.* **2019**, *7*, 102946. [[CrossRef](#)]
46. Zhou, Y.X.; Chen, Y.Z.; Hu, Y.; Huang, G.; Yu, S.H.; Jiang, H.L. MIL-101-SO₃H: A Highly Efficient Brønsted Acid Catalyst for Heterogeneous Alcoholysis of Epoxides under Ambient Conditions. *Chem. Eur. J.* **2014**, *20*, 14976–14980. [[CrossRef](#)]
47. Zhang, F.; Jin, Y.; Fu, Y.; Zhong, Y.; Zhu, W.; Ibrahim, A.A.; El-Shall, M.S. Palladium Nanoparticles Incorporated within Sulfonic Acid-Functionalized MIL-101(Cr) for Efficient Catalytic Conversion of Vanillin. *J. Mater. Chem. A Mater.* **2015**, *3*, 17008–17015. [[CrossRef](#)]
48. Santiago-Portillo, A.; Blandez, J.F.; Navalón, S.; Álvaro, M.; García, H. Influence of the Organic Linker Substituent on the Catalytic Activity of MIL-101(Cr) for the Oxidative Coupling of Benzylamines to Imines. *Catal. Sci. Technol.* **2017**, *7*, 1351–1362. [[CrossRef](#)]
49. Mehrabi, M.; Vatanpour, V.; Teber, O.O.; Masteri-Farahani, M.; Mortazavi, S.S.; Abbasi, A.; Koyuncu, I. Enhanced Negative Charge of Polyamide Thin-Film Nanocomposite Reverse Osmosis Membrane Modified with MIL-101(Cr)-Pyz-SO₃H. *J. Memb. Sci.* **2022**, *664*, 121066. [[CrossRef](#)]
50. Wang, Y.; Xie, Y.; Deng, M.; Liu, T.; Yang, H. Incorporation of Polyoxometalate in Sulfonic Acid-Modified MIL-101-Cr for Enhanced CO₂ Photoreduction Activity. *Eur. J. Inorg. Chem.* **2021**, *2021*, 681–687. [[CrossRef](#)]
51. Saikia, M.; Saikia, L. Sulfonic Acid-Functionalized MIL-101(Cr) as a Highly Efficient Heterogeneous Catalyst for One-Pot Synthesis of 2-Amino-4H-Chromenes in Aqueous Medium. *RSC Adv.* **2016**, *6*, 15846–15853. [[CrossRef](#)]
52. Yang, J.M.; Zhang, W.; Zhang, R.Z.; Tong, M.X. Modulation of the Driving Forces for Adsorption on MIL-101 Analogues by Decoration with Sulfonic Acid Functional Groups: Superior Selective Adsorption of Hazardous Anionic Dyes. *Dalton Trans.* **2020**, *49*, 6651–6660. [[CrossRef](#)]

Disclaimer/Publisher’s Note: The statements, opinions and data contained in all publications are solely those of the individual author(s) and contributor(s) and not of MDPI and/or the editor(s). MDPI and/or the editor(s) disclaim responsibility for any injury to people or property resulting from any ideas, methods, instructions or products referred to in the content.